UNIVERSITY OF LEEDS

Acoustic phonon modulation of terahertz quantum cascade lasers

A. Demic, A. Valavanis, J. Bailey, P. Dean, L. H. Li,
A. G. Davies, E. H. Linfield, P. Harrison,
J. E. Cunningham, A. Kent

The University of Nottingham
UNITED KINGDOM · CHINA · MALAYSIA

University of HUDDERSFIELD

Motivation

- THz QCLs – coherent THz sources based on resonant tunnelling transport in conduction band in periodic superlattice.
- Propagating acoustic strain pulse through 10 μm superlattice
- Modelling challenge: mix of phonon and electronic transport that breaks superlattice periodicity.

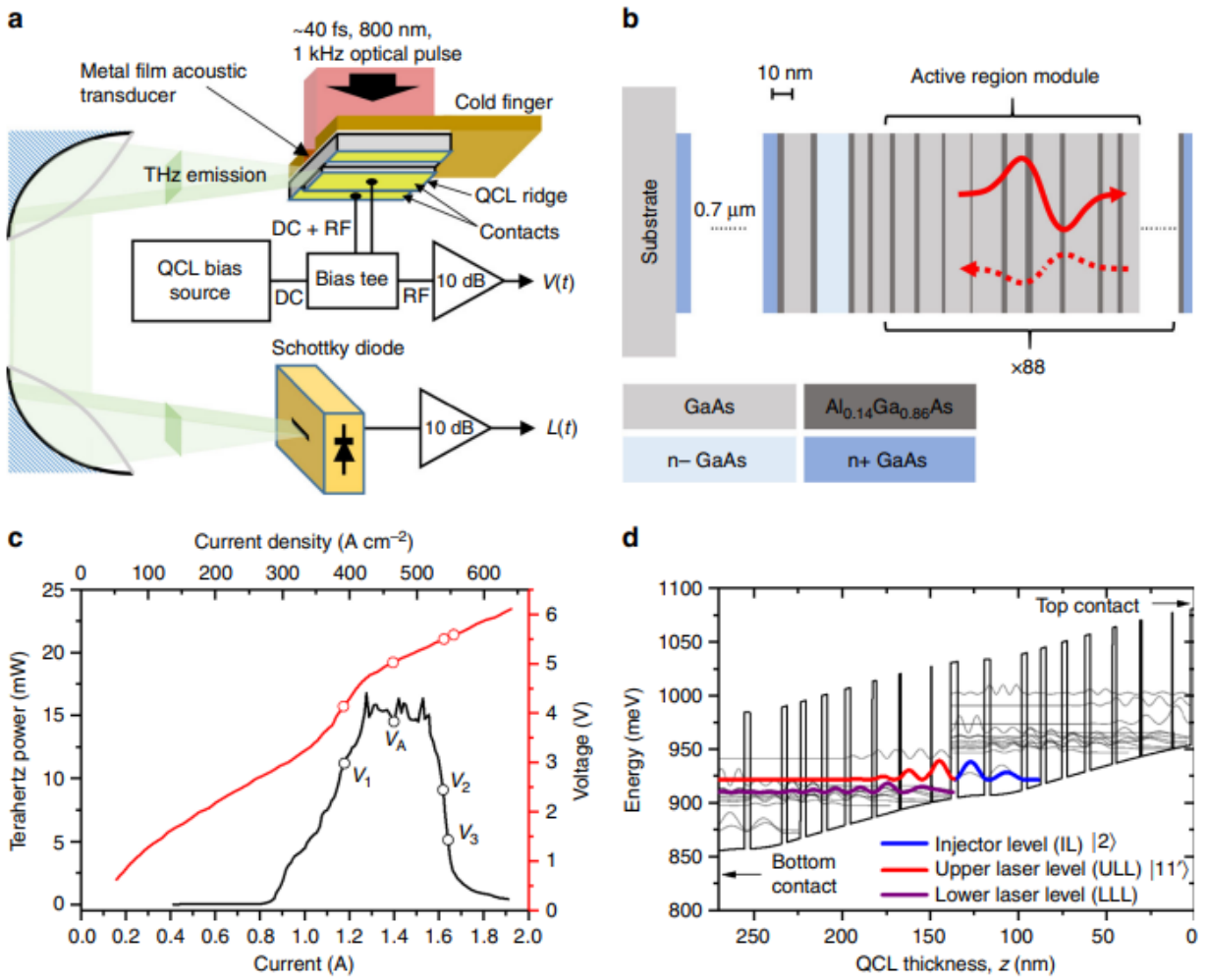

Fig. 1 Experimental arrangement and QCL device structure and characteristics. a Experimental arrangement for measuring the optical and electronic perturbation of a THz QCL by laser-generated picosecond acoustic pulses. The sample is mounted on the cold finger of an optical cryostat at an operating temperature of 15 K. **b** Schematic diagram of the QCL device structure showing the transmitted (solid red line) and reflected (dashed red line) strain pulses. **c** *L–I–V* characteristics of the QCL in the absence of acoustic pulses, measured at a temperature of ~10 K and driven with 50-μs pulses at a 1-kHz repetition rate. Labels correspond to the different QCL biasing conditions used in experiments: ($V_1 = 4.13$ V, $V_A = 5.02$ V, $V_2 = 5.49$ V and $V_3 = 5.58$ V). **d** Simplified QCL band structure showing two periods of the structure with labelled injection level (IL-|2⟩), upper laser level (ULL-|11′⟩) and lower lasing level (LLL). Source data for **c** and **d** are provided in ref. [50].

A. Dunn, C. Poyser, P. Dean, A. Demic, *et al.* High-speed modulation of a terahertz quantum cascade laser by coherent acoustic phonon pulses. *Nat Commun* **11**, 835 (2020).

Motivation

- Observed modulation ~160 MHz
- Potential modulation ~300 GHz
- Phenomenological theoretical explanation through time dependent Schrodinger perturbation theory:

$$c_n(t) = \delta_{ni} - \frac{i}{\hbar}\int_{t_0}^{t} dt'\, e^{i\omega_{ni}t'} V_{ni}(t') - \frac{1}{\hbar^2}\sum_m \int_{t_0}^{t} dt' \int_{t_0}^{t'} dt'' e^{i\omega_{nm}t' + i\omega_{mi}t''} V_{nm}(t') V_{mi}(t''),$$

$$V_{nm}(t) = < n|V|m >$$

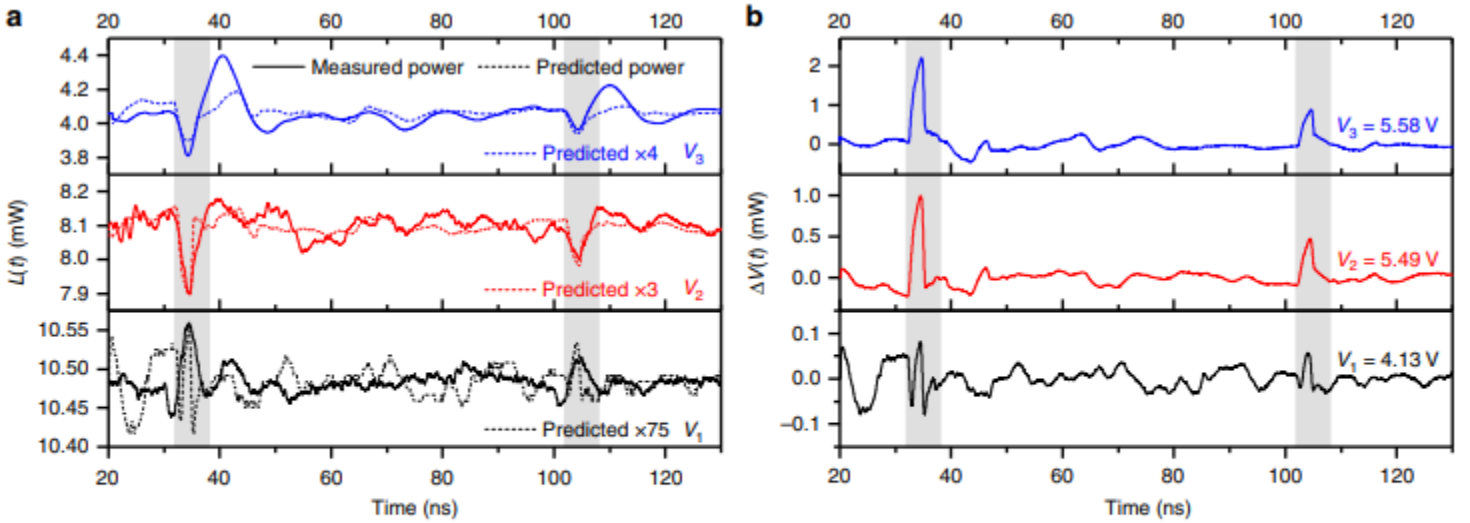

Fig. 3 Measurement and prediction of effect of the acoustic modulation. Temporal responses of the QCL to the first two strain pulses at three different QCL operating biases $V_b = V_1$ to V_3: **a** THz power modulation, $L(t)$ (solid lines) and **b** QCL voltage perturbation, $\Delta V(t)$. Predicted power modulation waveforms are shown in (**a**) (dashed lines), with amplitudes normalised to the experimental data by factors of 75, 3 and 4 for V_1, V_2 and V_3, respectively. Highlighted regions indicate the temporal position of the acoustic modulations. Incident strain pulses were generated with an optical pulse energy of 10 μJ. Data have been smoothed using a 20-point rolling average filter. Source data are provided as a Source Data file.

A. Dunn, C. Poyser, P. Dean, A. Demic, *et al.* High-speed modulation of a terahertz quantum cascade laser by coherent acoustic phonon pulses. *Nat Commun* **11**, 835 (2020).

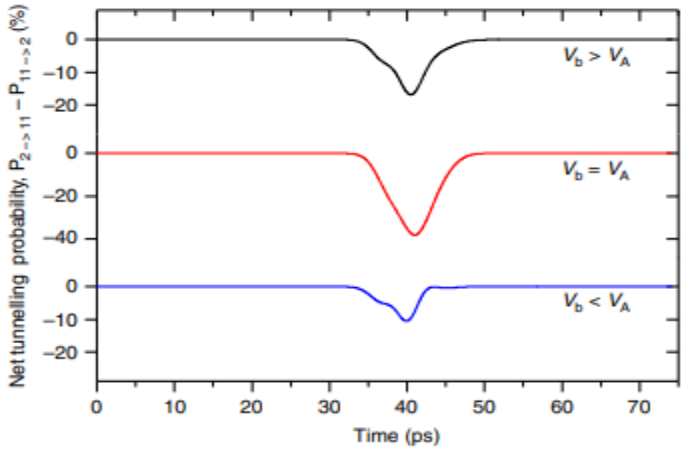

Fig. 5 Net tunnelling probabilities for the perturbed QCL device using a time-dependent model. Time-dependent net tunnelling probabilities between the injection level (|2⟩) and the upper laser level (|11′⟩) due to transit of the acoustic wave, calculated using a time-dependent perturbation model for QCL biases below subband alignment ($V_b < V_A$, $V_b = 3.53$ kV cm^{-1}), at alignment ($V_b = V_A$, $V_b = 3.63$ kV cm^{-1}) and above alignment ($V_b > V_A$, $V_b = 3.85$ kV cm^{-1}). The timescale of the simulation is set so that the pulse can propagate over two adjacent periods. Source data are provided as a Source Data file.

Acoustic phonons in superlattice

- Acoustic wave equation:

$$\frac{\partial}{\partial z} v_s^2(z) \frac{\partial}{\partial z} p(z,t) - \frac{\partial^2}{\partial t^2} p(z,t) = 0$$

- Fourier (slow envelope) approximation $p(z,t) = p_n(z) \exp(i\omega t)$:

$$-\frac{\partial}{\partial z} v_s^2(z) \frac{\partial}{\partial z} p_n(z,t) = \omega_n \, p_n(z,t)$$

- Quasi-analytical solution due to $v_s \ll \omega_n$:

$$\omega_{\text{bulk},n} = \frac{n\pi v_{\text{bulk}}}{d} \qquad \omega_{\text{avg},n} = \frac{n\pi}{\sum_l \frac{d_l}{v_l}} = \frac{1}{\sum_l \frac{1}{\omega_l}}$$

- We can define deviations from numerical solution as:

$$\Delta f_{\text{bulk},n} = f_n - \frac{n v_{\text{bulk}}}{2d}, \qquad \Delta f_{\text{avg},n} = f_n - \frac{n}{2\sum_l \frac{d_l}{v_l}}$$

Acoustic phonons in superlattice - experiment

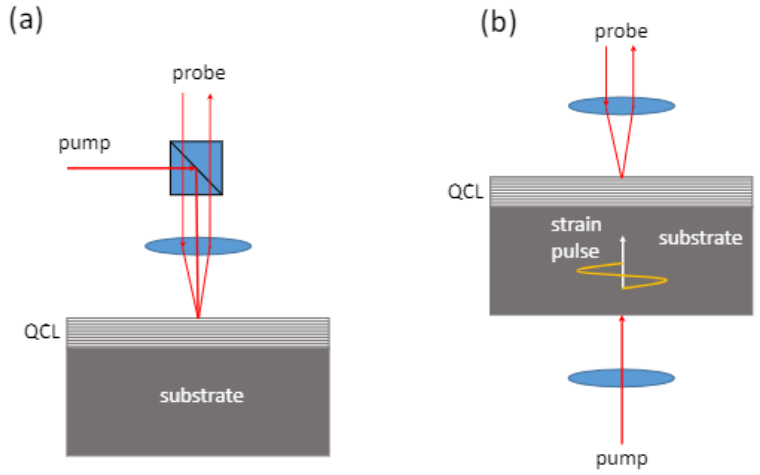

FIG. 1. Schematic illustrations of ASOPS experimental configurations, showing (a) reflection mode, and (b) transmission mode geometries.

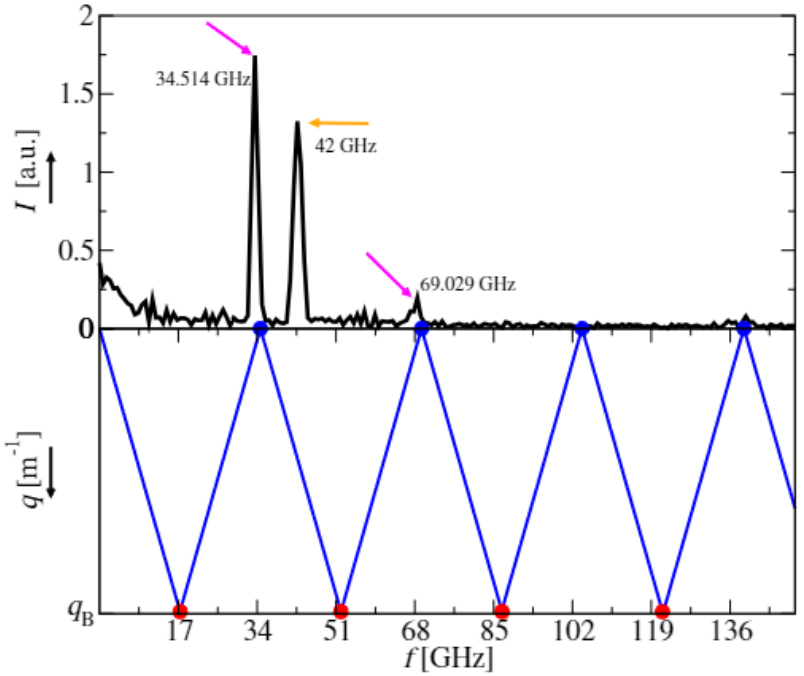

FIG. 2. Experimental probe reflectivity spectrum (top), obtained using a reflection-mode ASOPS geometry, and folded dispersion of the first Brillouin zone (bottom), obtained by solving Eq. (2) for a single period of the QCL. Blue and red circles indicate BZC and BZE modes respectively.

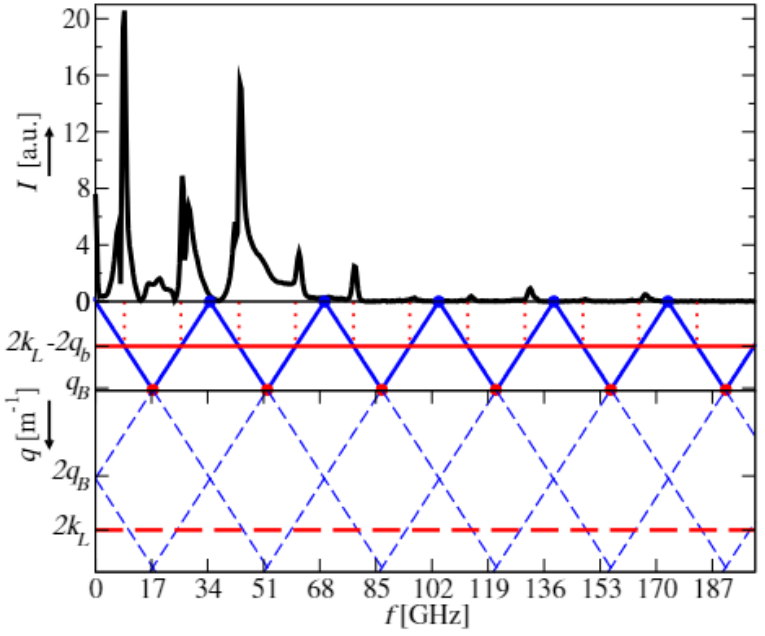

FIG. 3. Experimental probe reflectivity spectrum (top), using the configuration in Fig. 1(b), and acoustic dispersion resulting from model in Equation (2). Solid blue lines represent the phonon dispersion, folded into the first Brillouin zone, while dashed lines represent the extended dispersion at higher phonon wave vectors. The red dashed line corresponds to $q = 2k_{\mathrm{L}}$, and the red solid line shows this folded into the first phonon Brillouin zone.

Acoustic phonons in THz QCLs

Structure.	Layer thicknesses [Å]	Al composition in $Al_xGa_{1-x}As$ layers
Device A	106/**5**/170/**10**/135/**21**/124/**31**/100/**31**/90/**31**/75/**31**/178/**31**/152/**41**	$x = 0.14$
Device B	110/**18**/115/**35**/94/**39**/184/**48**	$x = 0.15$
Device C	144/**10**/118/**10**/144/**24**/144/**24**/132/**30**/124/**32**/120/**44**/126/**50**	$x = 0.1$
Device D	76.4/**17.5**/154.7/**33.7**	$x = 0.3$
Device E	82/**46**/72/**41**/160/**43**	$x = 0.15$, $x = 0.075$
Device F	$x(z) = \frac{4x_0}{d_{sl}^2}\left(z - \frac{d_{sl}}{2}\right)^2$	$d_{sl} = 3000$ Å, $dz = 2.825$ Å , $x_0 = 0.14$
Device G	$x(z) = \frac{4x_0}{d_{sl}^2}\left(z - \frac{d_{sl}}{2}\right)^2\left[1 + 0.18 \cdot \frac{4x_0}{d_{sl}^2}\left(z - \frac{d_{sl}}{2}\right)^2\right]$	$d_{sl} = 620$ Å, $dz = 2.825$ Å , $x_0 = 0.42$
Device H	42/**17**/20/**17**	$x = 1$
Device D_1	76.4/**35**/154.7/**33.7**	$x = 0.3$
Device C_1	144/**10**/118/**10**/144/**24**/144/**24**/132/**30**/124/**32**/120/**44**/126/**50**	$x = 0.1$, $x = 1$
Device C_2	144/**10**/118/**10**/144/**24**/144/**24**/132/**30**/124/**32**/120/**44**/126/**50**	$x = 0.1$, $x = 1$
Device A_1	106/**5**/170/**10**/135/**21**/124/**31**/100/**31**/90/**31**/75/**31**/178/**31**/152/**41**	$x = 0.14$, $x = 0.3$
Device I	150/**20**/150/**40**/150/**80**	$x = 1$
Device J	100/**20**/100/**20**/200/**20**/200/**20**	$x = 0.1$

- THz QCL types:
  - Bound-to-continuum – 8 - 15 wells, low barriers, all states need to be <36 meV
  - Resonant (LO) phonon – 2 – 4 wells, lower laser levels is depopulated by 36 meV transition
  - Hybrid – 8 – 15 wells, mix of former two (LO transition is added below miniband)

Acoustic phonons in THz QCLs

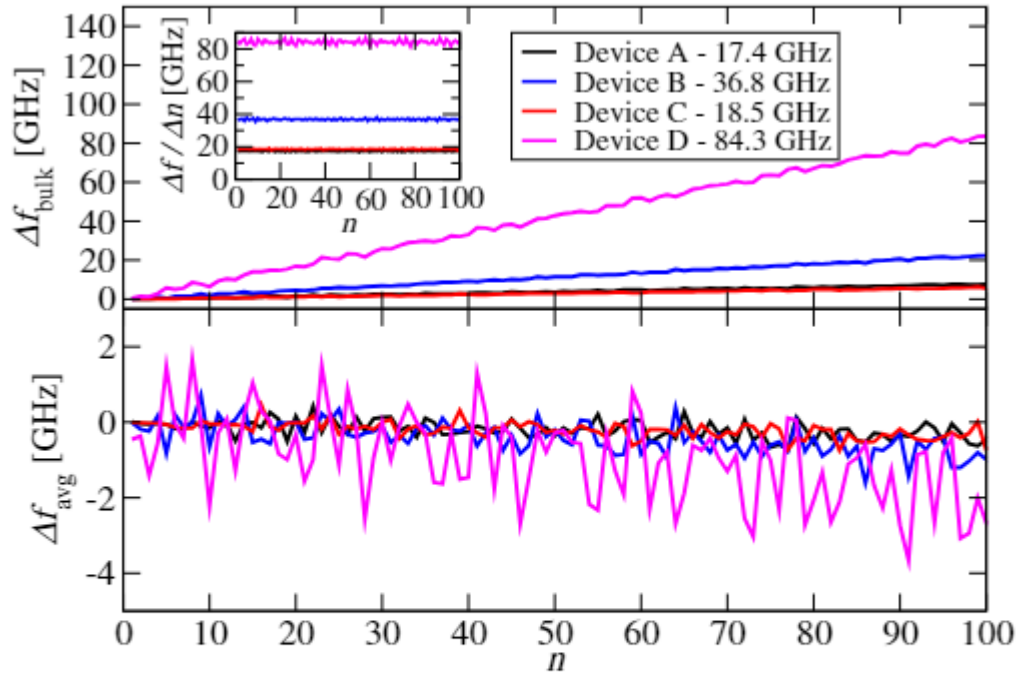

FIG. 4. Frequency offset from the bulk (top) and average (bottom) approximation calculated by Eq. (11) for QCL devices A–D. Inset: the frequency difference between consecutive resonant acoustic modes for the corresponding structures.

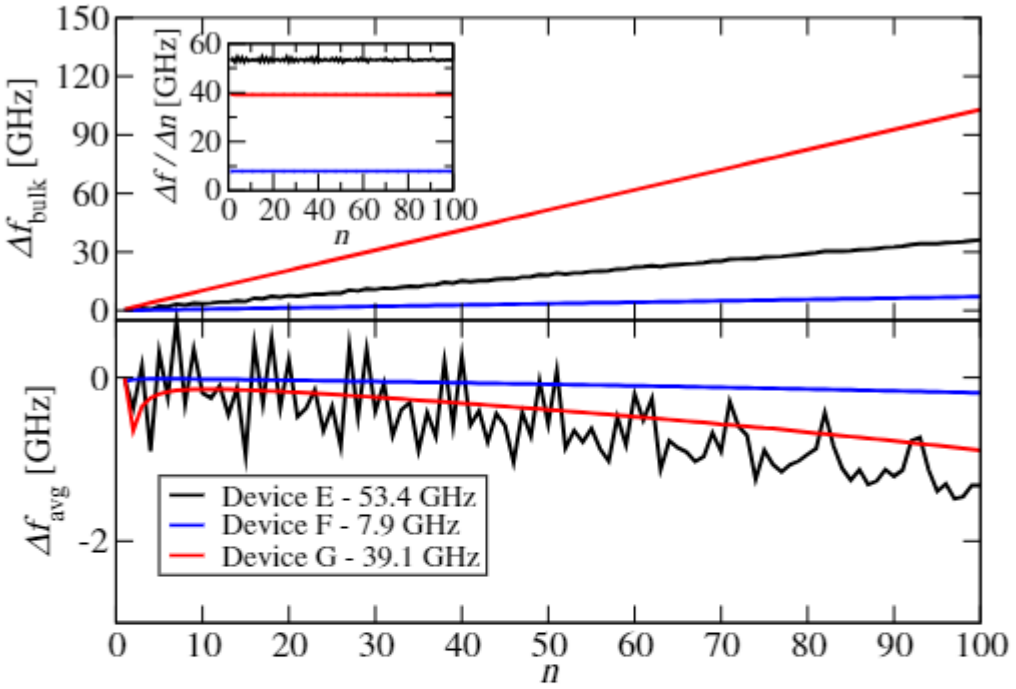

FIG. 5. Frequency offset from the bulk (top) and average (bottom) approximation calculated by Eq. (11) for variable barrier height LO phonon THz QCL structure [37] (Device E), a parabolic quantum well superlattice (Device F) that quadratically varies Al content $x = 0 - 0.14$ across 3000 Å period length and a parabolic quantum well (Device G) with varying Al content $x = 0 - 0.42$ across 620 Å well length. We used a mono-layer step of 2.825 Å for generating the parabolic profiles. Inset: the frequency difference between consecutive resonant acoustic modes for the corresponding structures.

Acoustic phonons in THz QCLs – fine structure

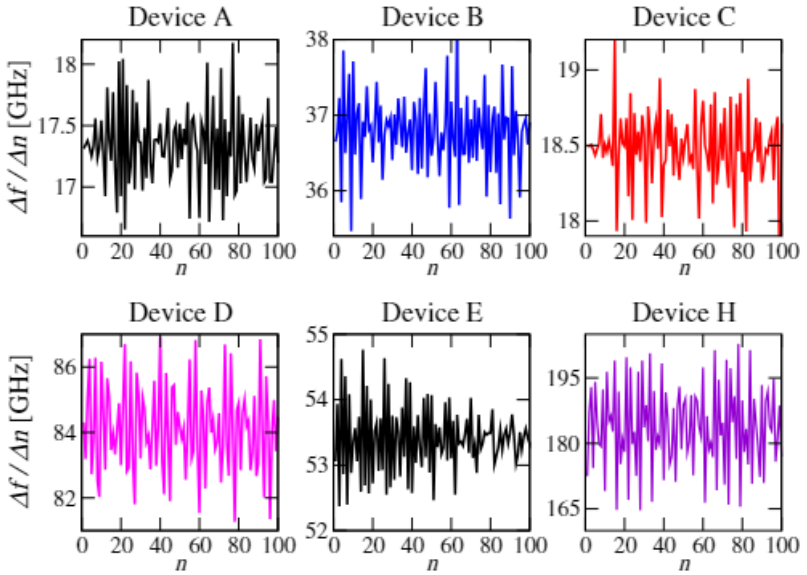

FIG. 6. The frequency difference between consecutive resonant acoustic modes for the corresponding structures analysed in this section.

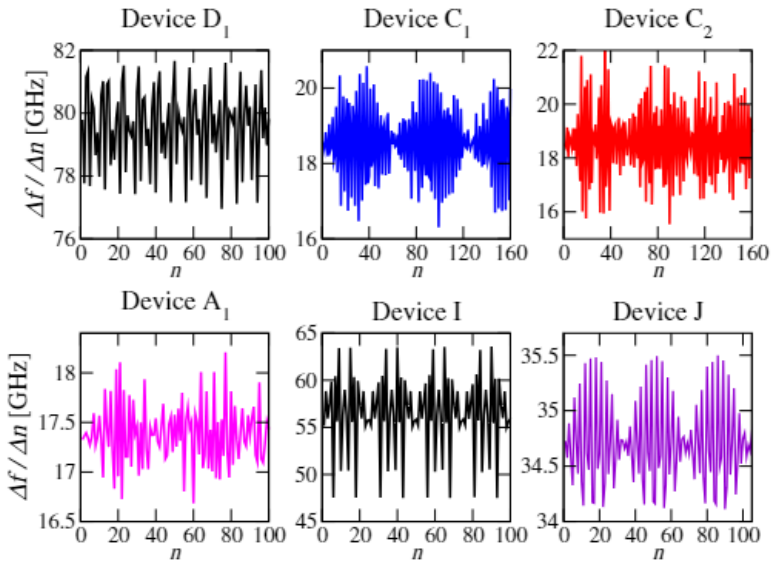

FIG. 7. The frequency difference between consecutive resonant acoustic modes for altered structures that test validity of approximation created by Eq. (13)

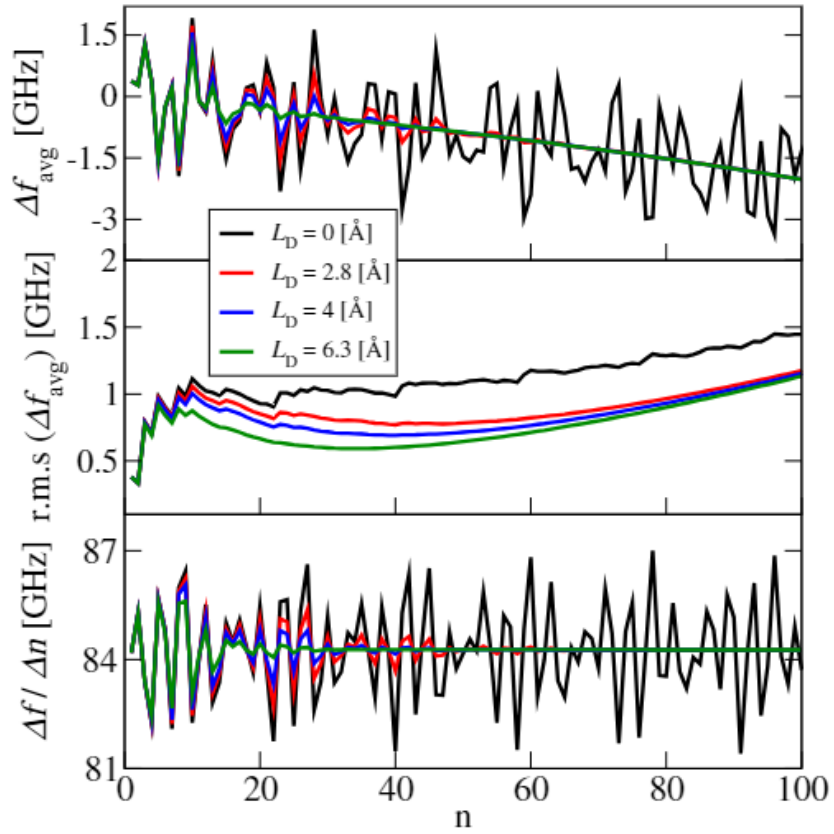

FIG. 8. We analyse Structure D for several values of diffusion length using the annealing model in [40]. Top and middle: Frequency offset from the average approximation [Eq. (11)] and its cumulative root mean square average, respectively. Bottom: The frequency difference between consecutive resonant modes.

Acoustic phonons in THz QCLs – transport modulation

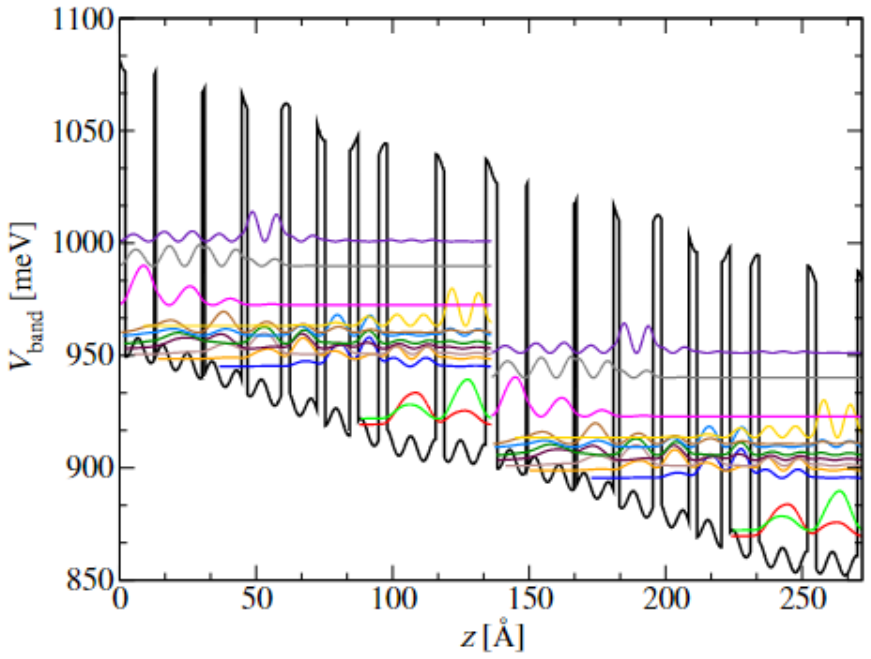

FIG. 9. Conduction band potential of a hybrid QCL design [28] with the addition of the 30th acoustic mode with modulation $M = 5$ meV. Two periods are shown at the resonance bias $K = 3.63\,\mathrm{kV\,cm^{-1}}$ along with the corresponding wavefunction moduli squared.

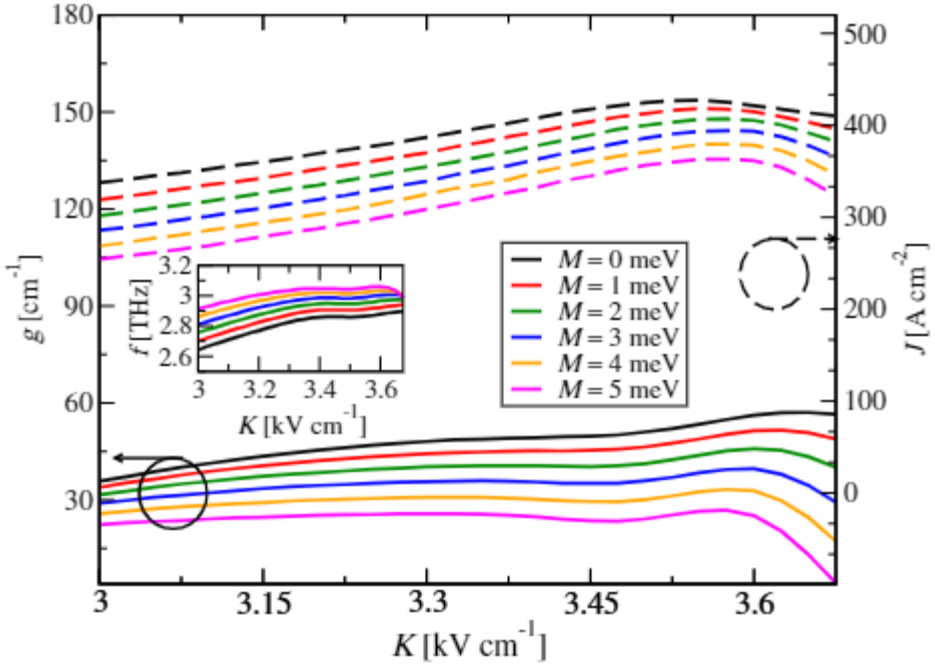

FIG. 10. Material gain and current density dependence on electric field when the first acoustic mode $n = 1$ is added with a range of modulation strengths to the conduction band potential of Device A.

- Acoustic wave envelopes are directly proportional to deformation potential and strain, thus the strain should linearly add to bandstructre potential, hence we can define modulation perturbation as:

$$H' = Mp_n(z)$$

Acoustic phonons in THz QCLs – modulation strength

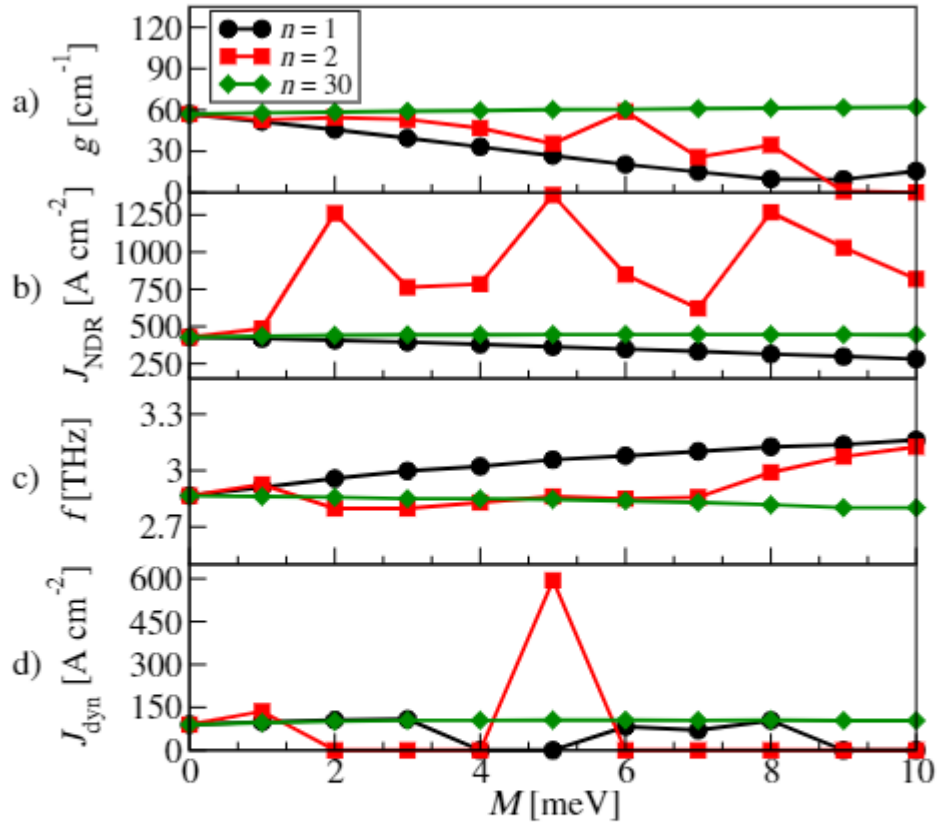

FIG. 11. Dependence of performance parameters for Device A, as a function of modulation strength using acoustic modes $p_n(z)$ with indices $n = 1, 2, 30$. Results are shown for (a) peak gain, (b) current density at the NDR point, (c) emission frequency (at NDR point) and (d) dynamic range.

- Somewhat inconclusive effect as low modes behave differently than the higher modes.
- Higher modes show negligible effect on transport even at very high (and unphysical) modulation strengths.

Acoustic phonons in THz QCLs – mode number

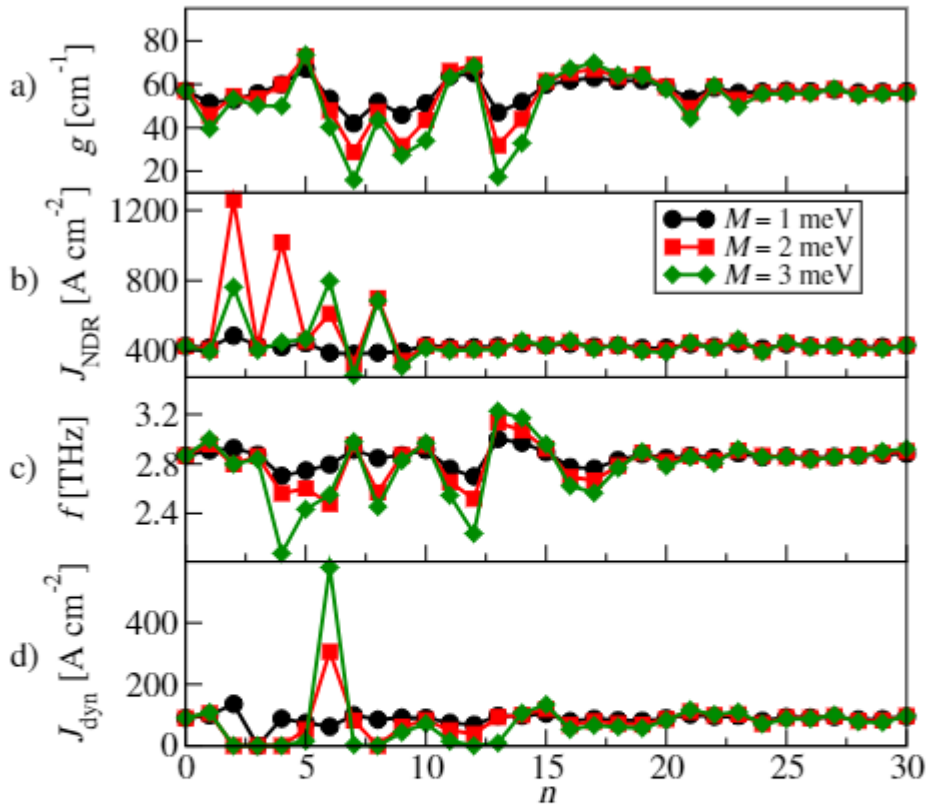

FIG. 12. Dependence of performance parameters for Device A (Hybrid QCL design), as a function of acoustic mode $p_n(z)$ index, using varying modulation strengths $M = 1, 2, 3$ meV. Results are shown for (a) peak gain, (b) current density at the NDR point, (c) emission frequency at NDR point and (d) dynamic range. Values corresponding to $n = 0$ represent non-perturbed values (ie $M = 0$).

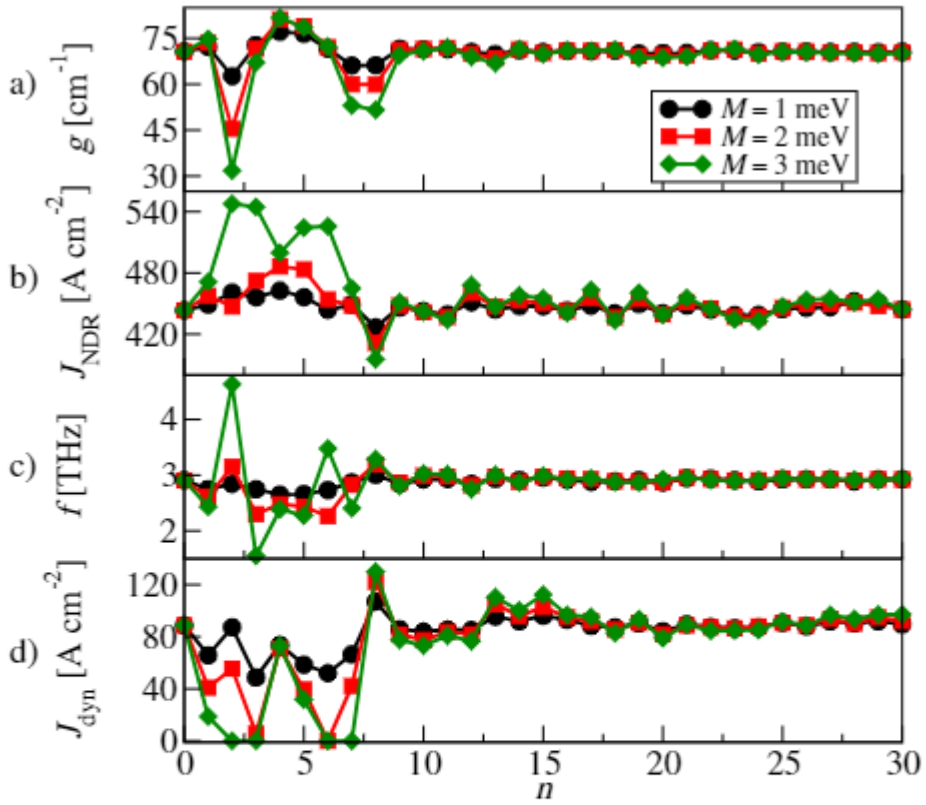

FIG. 13. Dependence of performance parameters for Device B(LO phonon design), as a function of acoustic mode $p_n(z)$ index, using varying modulation strengths $M = 1, 2, 3$ meV. Results are shown for (a) peak gain, (b) current density at the NDR point, (c) emission frequency (at NDR point) and (d) dynamic range.

Acoustic phonons in THz QCLs – mode number

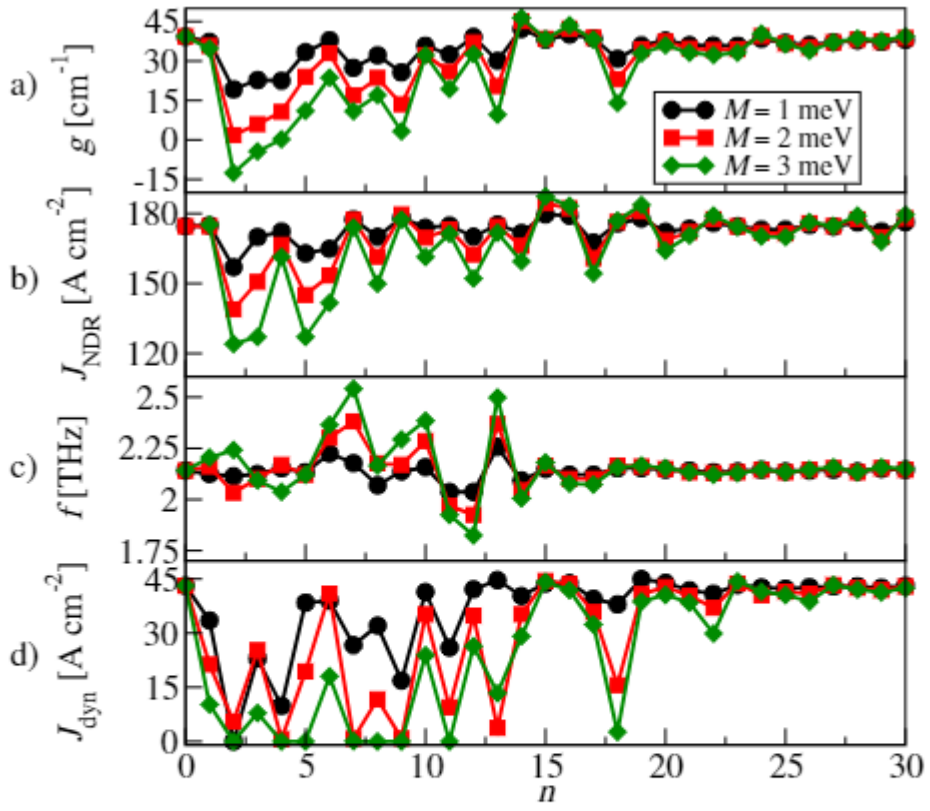

FIG. 14. Dependence of performance parameters for Device C (BTC design), as a function of acoustic mode $p_n(z)$ index, using varying modulation strengths $M = 1, 2, 3$ meV. Results are shown for (a) peak gain, (b) current density at the NDR point, (c) emission frequency (at NDR point) and (d) dynamic range.

- Higher modes oscillate at much smaller length scales than the superlattice layers
- The perturbation with higher modes acts as adding a constant to Schrodinger equation – thus no effect even at unrealistic modulation strengths.
- Longer period superlattices are more sensitive to modulation
- Modulation is highly sensitive up to ~200 GHz regardless on THz QCL design